Modéliser notre environnement : comment aller au-delà des capacités de calcul actuelles.

Catherine Choquet

Journées Portes Ouvertes 2013

9 février 2013 - La Rochelle

Où se cachent les maths ?

une combinaison non homologuée...

Proof: We multiply Equation (7) by an admissible test function in the form $\varepsilon^4\phi(x,Z,x/\varepsilon^2)$ and we integrate by parts. Using in particular $h^{-1}\Delta h - h^{-2}|\nabla h|^2 = \mathrm{div}(h^{-1}\nabla h)$, we get

$$
\begin{aligned}
0 = &\int_\Omega \nabla_x u^\varepsilon \cdot (\varepsilon^4\nabla_x\phi^\varepsilon + \varepsilon^2\nabla_X\phi^\varepsilon)\,dx\,dZ \\
&- \int_\Omega \varepsilon^4(\nabla_x h_1 + \varepsilon^{-1}(1-\psi^\varepsilon)\nabla_X h_2^\varepsilon - \varepsilon^{1-\alpha}h_2^\varepsilon\nabla_x\psi^\varepsilon)\cdot\frac{1}{h_1+\varepsilon(1-\psi^\varepsilon)h_2^\varepsilon} \\
&\qquad \Big(\nabla_x u^\varepsilon\partial_Z(Z\phi^\varepsilon) + Z\partial_Z u^\varepsilon(\nabla_x\phi^\varepsilon + \frac{1}{\varepsilon^2}\nabla_X\phi^\varepsilon)\Big)\,dx\,dZ \\
&+ \int_\Omega \varepsilon^4\frac{|\nabla_x h_1 + \varepsilon^{-1}(1-\psi^\varepsilon)\nabla_X h_2^\varepsilon - \varepsilon^{1-\alpha}h_2^\varepsilon\nabla_x\psi^\varepsilon|^2}{|h_1+\varepsilon(1-\psi^\varepsilon)h_2^\varepsilon|^2}\partial_Z u^\varepsilon\cdot[\partial_Z(Z^2\phi^\varepsilon) - Z\phi^\varepsilon]\,dx\,dZ \\
&+ \int_\Omega \varepsilon^2\frac{1}{|h_1+\varepsilon(1-\psi^\varepsilon)h_2^\varepsilon|^2}\partial_Z u^\varepsilon\cdot\partial_Z\phi^\varepsilon\,dx\,dZ - \int_\Omega \varepsilon^2 p^\varepsilon(\varepsilon^2\mathrm{div}_x\phi^\varepsilon + \mathrm{div}_X\phi^\varepsilon)\,dx\,dZ \\
&+ \int_\Omega \varepsilon^2(\nabla_x h_1 + \varepsilon^{-1}(1-\psi^\varepsilon)\nabla_X h_2^\varepsilon - \varepsilon^{1-\alpha}h_2^\varepsilon\nabla_x\psi^\varepsilon)\cdot\frac{1}{h_1+\varepsilon(1-\psi^\varepsilon)h_2^\varepsilon}\varepsilon^2 p^\varepsilon\partial_Z(Z\phi^\varepsilon)\,dx\,dZ.
\end{aligned}
$$

We recall that $\|\nabla_x u^\varepsilon\|_{(L^2(\Omega))^{(d-1)\times(d-1)}} \le C\varepsilon^{1-\alpha}$ and $\|\partial_Z u^\varepsilon\|_{(L^2(\Omega))^{d-1}} \le C$. If $\alpha < 3$, we check straightforward that all the terms containing the velocity u^ε disappear when $\varepsilon \to 0$ in the former relation. Since $\alpha \ge \beta$, this is a particular case of the assumption $\{3\alpha+\beta<12\}$.

We now consider the general case $\{3\alpha+\beta<12\}$. Let us focus on the main order terms of each line in the right hand side of (21). Due to Estimate (11), for any $p \ge 1$,

$$
\|\varepsilon^2\nabla_x u^\varepsilon\|_{L^p} \le C\varepsilon^{\frac{6p-2\beta+2\alpha-(3\alpha-\beta)p}{2p}} + C\varepsilon = C\varepsilon^{r_u(p)/2p} + C\varepsilon,
$$

where function r_u was defined in the proof of Lemma 4.1. It was shown that, if $(\alpha+\beta<6)$, there exists $p_u > 1$ such that $r_u(p_u) > 0$ and then $\lim_{\varepsilon\to 0}\|\varepsilon^2\nabla_x u^\varepsilon\|_{L^{p_u}} = 0$. It follows that

$$
\lim_{\varepsilon\to 0}\int_\Omega \nabla_x u^\varepsilon\cdot(\varepsilon^4\nabla_x\phi^\varepsilon + \varepsilon^2\nabla_X\phi^\varepsilon) = 0.
$$

For the next terms, following for instance the lines of the proof of Lemma 2.1, we compute:

$$
\|\nabla_x\psi(x/\varepsilon^\alpha)\|_{L^q} \le C\varepsilon^{-\alpha}\varepsilon^{\frac{\alpha-\beta}{q}}. \tag{22}
$$

Thus the main order terms in the next four lines of (21) are such that

$$
\begin{array}{ll}
\|\varepsilon^{5-\alpha}\nabla_x\psi^\varepsilon\cdot\nabla_x u^\varepsilon\|_{L^p} \le \varepsilon^{5-\alpha}\|\nabla_x u^\varepsilon\|_{L^2}\|\nabla_x\psi^\varepsilon\|_{L^{2p/(2-p)}}, & \|\varepsilon^{5-\alpha}\nabla_x\psi^\varepsilon\cdot\nabla_x u^\varepsilon\|_{L^1} \le C\varepsilon^{6-3\alpha/2-\beta/2}, \\
\|\varepsilon^{3-\alpha}\nabla_x\psi^\varepsilon\cdot\partial_Z u^\varepsilon\|_{L^p} \le \varepsilon^{3-\alpha}\|\partial_Z u^\varepsilon\|_{L^2}\|\nabla_x\psi^\varepsilon\|_{L^{2p/(2-p)}}, & \|\varepsilon^{3-\alpha}\nabla_x\psi^\varepsilon\cdot\partial_Z u^\varepsilon\|_{L^1} \le C\varepsilon^{3-\alpha/2-\beta/2}, \\
\|\varepsilon^{6-2\alpha}\nabla_x\psi^\varepsilon\cdot\partial_Z u^\varepsilon\|_{L^p} \le \varepsilon^{6-2\alpha}\|\partial_Z u^\varepsilon\|_{L^2}\|\nabla_x\psi^\varepsilon\|_{L^{2p/(2-p)}}, & \|\varepsilon^{6-2\alpha}\nabla_x\psi^\varepsilon\cdot\partial_Z u^\varepsilon\|_{L^1} \le C\varepsilon^{6-3\alpha/2-\beta/2}, \\
\|\varepsilon^{5-\alpha}\nabla_x\psi^\varepsilon p^\varepsilon\|_{L^p} \le \varepsilon^{3-\alpha}\|\varepsilon^2 p^\varepsilon\|_{L^2}\|\nabla_x\psi^\varepsilon\|_{L^{2p/(2-p)}}, & \|\varepsilon^{5-\alpha}\nabla_x\psi^\varepsilon p^\varepsilon\|_{L^1} \le C\varepsilon^{3-\alpha/2-\beta/2}.
\end{array}
$$

The work then consists in introducing auxiliary functions of the Lebesgue exponent $p \in (1,2)$ and linked with the powers of ε in the estimates below. We then study their variations as in the proof of Lemma 4.1. Here, instead of detailing all these computations, we have written the L^1-estimates

Où se cachent les maths ?

Le début de l'histoire

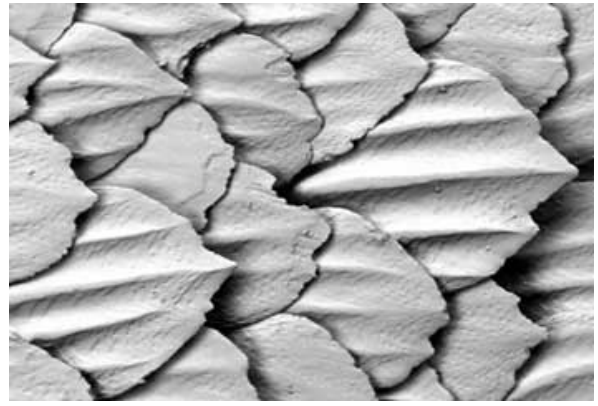

- Biomimétique.
- 250 records du monde de natation en 2008.
- America's cup.
- Applications militaires...

Observations physiques

Effet “riblet” : rugosité, tourbillons et diminution de la résistance au fluide.

Augmentation de la pression dans une mince couche de fluide.

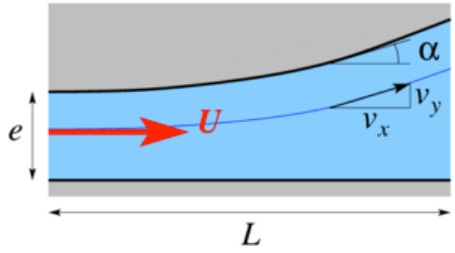

Dans un cadre plus prosaïque

À l'échelle microscopique :

Réarrangement des particules :

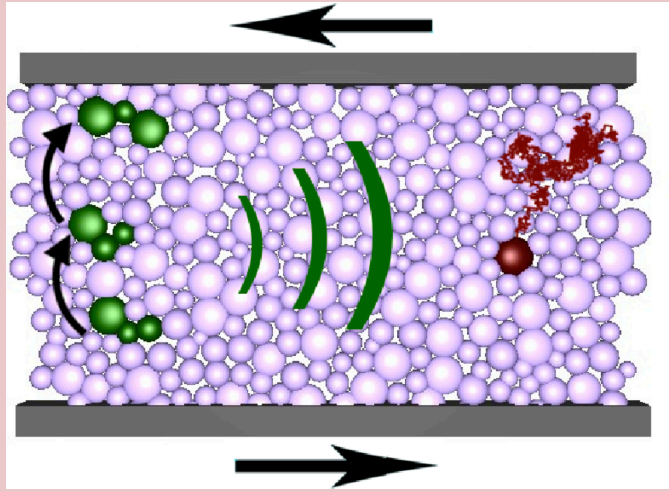

Hors de nos capacités de calcul !

À l'échelle du continu :

Équations de Navier-Stokes :

$$\partial_t \rho + \nabla \cdot (\rho \vec{v}) = 0,$$
$$\partial_t (\rho \vec{v}) + \nabla \cdot (\rho \vec{v} \times \vec{v}) = -\nabla p + \nabla \cdot \tau + \rho \vec{f},$$
$$\partial_t (\rho e) + \nabla \cdot ((\rho e + p)\vec{v}) = \nabla \cdot (\tau \vec{v})$$

Un des problèmes du millénaire (1 million de dollars) : inmaitrisable numériquement !

Enfin un modèle manipulable à l'échelle du continu :

Approximation de Reynolds (1889) :

$$\nabla_x \cdot \left(\frac{\overline{h}^3}{6} \nabla_x p \right) = \nabla_x (\overline{h} u_b).$$

- Enfin un modèle manipulable !
- Puisqu'il s'agit d'une approximation, que vaut l'erreur ?
- Où sont les effets de la rugosité ?

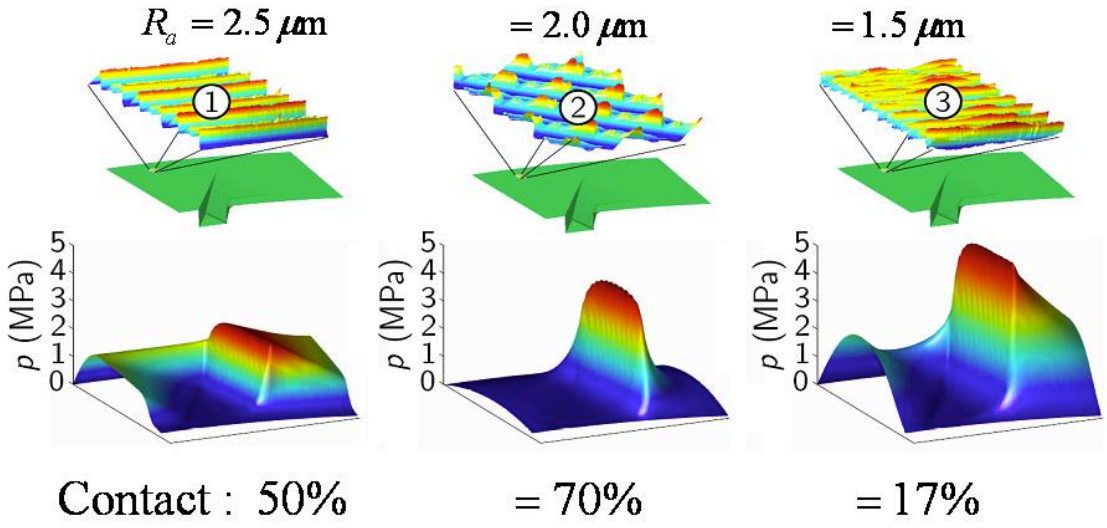

Justification du modèle de Reynolds avec rugosité

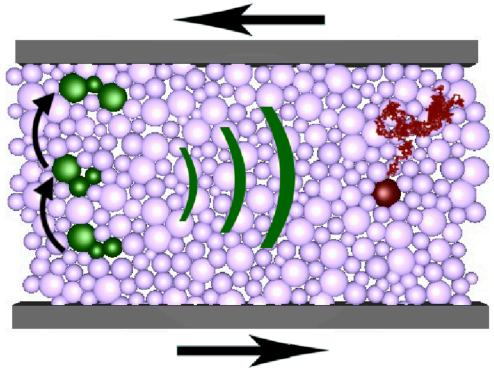

Changements d'échelles :

1. **de l'échelle des particules à l'échelle du continu ;**
2. **du continu 3D au continu 2D.**

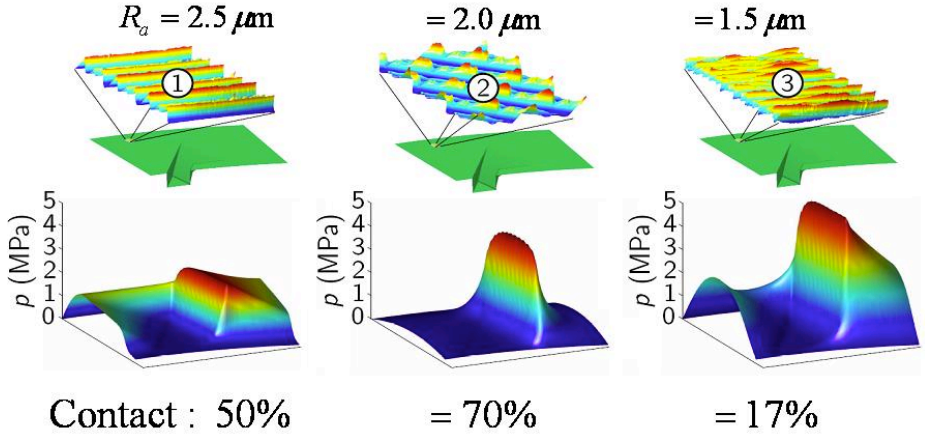

L'apport des mathématiques

Reconstruction de la peau de requin

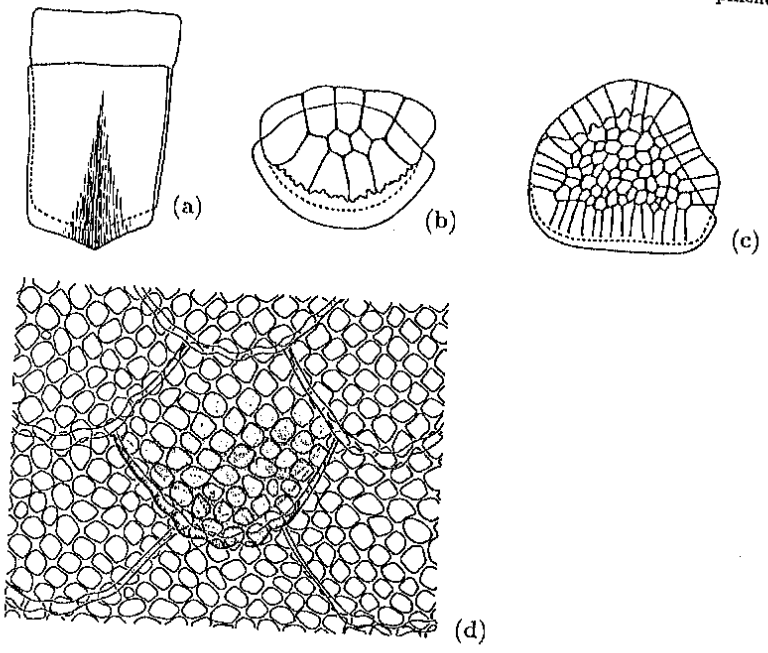

Fig. 17.25a-d. Examples of the different relationship between the osteoderms (bony dermal plates) and the overlying horny epidermal scales (after Otto 1908). (a) The dorsal region of the girdle-tailed lizard *Zonurus cordylus*. (b) The dorsal caudal (tail) region in the skink (a small lizard) *Chalcides* (*Gongylus*) *ocellatus* of the family *Scincidae*. (c) The region near the cloaca (anus) of the apotheker or "pharmacist' skink *Scincus officinalis*. (d) The ventral region of the common gecko, *Tarentola mauritanica*; here we have sha

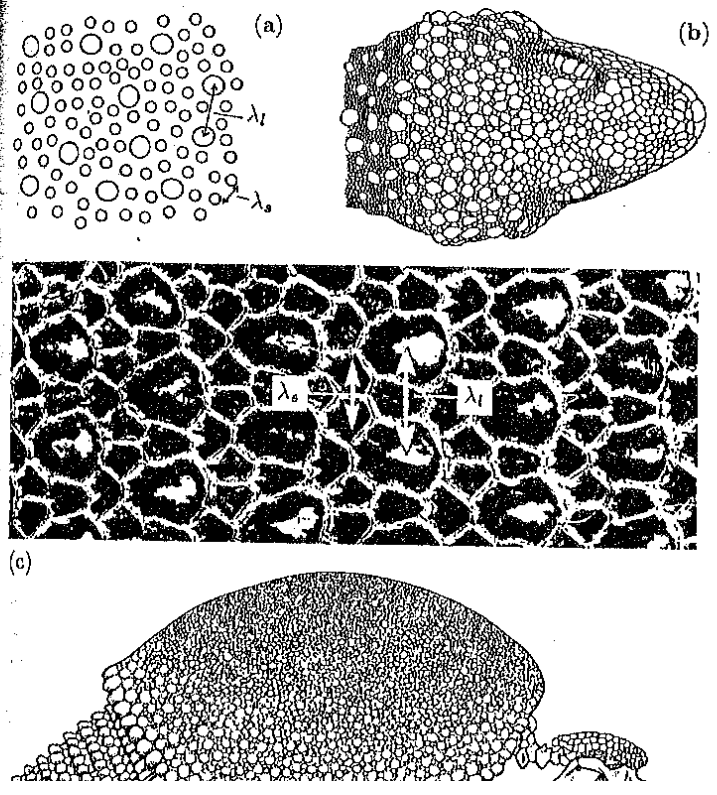

L'apport des mathématiques

Reconstruction de la peau de requin

where

$$f(G,\varepsilon) = -\sigma_0 + \frac{\pi}{1+\varepsilon} - \frac{G_T}{1+\varepsilon^2} - G\varepsilon\,,$$
$$g(G,\varepsilon) = k_+(\varepsilon) - [k_+(\varepsilon) + k_-(\varepsilon)]G\,, \qquad (17.104)$$

where the qualitative forms of $k_+(\varepsilon)$ and $k_-(\varepsilon)$ are shown in Fig. 17.23 (a).

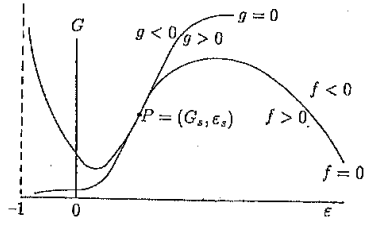

Fig. 17.24. Null clines $f(G,\varepsilon) = 0$, $g(G,\varepsilon) = 0$ for the strain-gel 'reaction diffusion' system (17.103) with (17.104) with parameter values such that the system can generate steady state spatial heterogeneous patterns in G and ε.

The 'reaction diffusion' system (17.103) with (17.104) is similar to those studied in depth in Chapters 12–15 and so we already know the wide range of pattern formation potential. Although in most of these analyses there was no convection, its presence simply enhances the steady state and wave pattern formation capabilities of the system. Typical nullclines $f = 0$ and $g = 0$ are illustrated in Fig. 17.24. Note that there is a nontrivial steady state (ε_s, G_s). Note also that the strain 'reactant' ε can be negative; it is bounded below by $\varepsilon = -1$.

If we linearize the system about the steady state as usual by writing

$$(w,v) = (G - G_s, \varepsilon - \varepsilon_s) \propto \exp[\lambda t + ikx]\,,$$

and substitute into the linearized system from (17.103), namely

$$G_s v_t = G_s v_{xx} + f_G w + f_\varepsilon v\,,$$
$$w_t + G_s v_t = D w_{xx} + g_G w + g_\varepsilon v\,,$$

where the partial derivatives of f and g are evaluated at the steady state (G_s, ε_s), we get the dispersion relation $\lambda(k^2)$ as a function of the wavenumber k. It is given by the roots of

$$G_s\lambda^2 + b(k)\lambda + d(k) = 0\,,$$

To get spatially heterogeneous structures we require

$$\begin{aligned} &\mathrm{Re}\,\lambda(0) < 0 \quad \Rightarrow \quad b(0) > 0, \quad d(0) > 0 \\ &\mathrm{Re}\,\lambda(k) > 0 \quad \Rightarrow \quad b(k) < 0 \ \text{ and/or } \ d(k) < 0 \ \text{ for some } \ k \neq 0\,. \end{aligned} \qquad (17.109)$$

The first of these in terms of the f and g derivatives at the steady state requires

$$-[f_\varepsilon + G_s g_G - G_s f_G] > 0, \quad f_\varepsilon g_G - f_G g_\varepsilon > 0\,. \qquad (17.110)$$

From Fig. 17.24 we see that

$$f_\varepsilon > 0, \quad f_G < 0, \quad g_\varepsilon > 0, \quad g_G < 0\,, \qquad (17.111)$$

and so (17.110) gives specific conditions on the parameters in f and g in (17.104). For spatial instability we now require the second set of conditions in (17.109) to hold. Because of the first of (17.110) it is not possible for $b(k)$ in (17.108) to be negative, so the only possibility for pattern is if $d(k)$ can become negative. This can happen only if the coefficient of k^2 is negative and the minimum of $d(k)$ is negative. This gives the conditions on the parameters for spatially unstable modes as

$$Df_\varepsilon + G_s g_G > 0\,,$$
$$(Df_\varepsilon + G_s g_G)^2 - 4G_s D(f_\varepsilon g_G - f_G g_\varepsilon) > 0\,, \qquad (17.112)$$

together with (17.110). The forms of f and g as functions of G and ε are such that these conditions can be satisfied.

From Chapter 14 we know that such reaction diffusion systems can generate a variety of one-dimensional patterns and in two dimensions, hexagonal structures. Although here we have only considered the one-dimensional model, the two-dimensional space system can indeed generate hexagonal patterns. Another scenario for generating hexagonal patterns, and one which is, from the viewpoint of generating a regular two-dimensional pattern, a more stable process, is if the patterns are formed sequentially as they did in the formation of feather germs in Section 17.5, with each row being displaced half a wavelength.

Let us now return to the formation of the microvilli and Fig. 17.22. The tension generated by the actomyosin fibres aligns the gel along the directions of stress. Thus the contracting gel forms a tension structure consisting of aligned fibres in a hexagonal array. Now between the dense regions the gel is depleted and less able to cope with the osmotic swelling pressure, which is always present in the cell interior. The suggestion, as mentioned at the beginning of this section, then is that this pressure pushes the sheet, at these places, into incipient